Journal of Cleaner Production 305 (2021) 127176

Contents lists available at ScienceDirect

Journal of Cleaner Production

journal homepage: www.elsevier.com/locate/jclepro

Mercury (II) ion adsorption performance of Cl-loaded carbonaceous material prepared by chlorination of pyrolyzed rice husk char

Yuuki Mochizuki, Javzandolgor Bud, Jiaqian Liu, Miki Takahashi, Naoto Tsubouchi*

Center for Advanced Research of Energy and Materials, Faculty of Engineering, Hokkaido University, Kita 13 Nishi 8, Kita-ku, Sapporo, 060-8628, Japan

ARTICLE INFO

Article history:
Received 30 September 2020
Received in revised form
9 March 2021
Accepted 16 April 2021
Available online 20 April 2021

Handling editor: Prof. Jiri Jaromir Klemeš

Keywords:
Rice husk
Mercury
Adsorption
Chlorination
Chlorine
Carbon

ABSTRACT

The objective of this study was to elucidate in detail the Hg adsorption performance of Cl-loaded carbons obtained after chlorination of rice husk char (RC). Firstly, chlorine content/morphology/porosity of Cl-loaded carbons prepared were investigated. Subsequently, Hg adsorption performance of Cl-loaded carbon was tested. The effect of Cl on Hg adsorption was then investigated by comparing the adsorption performance of Cl-loaded carbons prepared from RC and demineralized RC (DRC). Cl content of RC and DRC reached a maximum value at 600 °C, and then decreased by 1000 °C. The pore properties of RC chlorinated residue increased with increasing chlorination temperature. The Hg adsorption performance of the RC chlorinated residues increased with increasing chlorination temperature. The maximum Hg adsorption capacity of RC chlorinated residue obtained at 1000 °C, 10min reached 620 mg/g; the capacity of chlorinated residue treated with DRC at 1000 °C, 10min was larger than that of DRC chlorinated at 600 °C, which is largest Cl content. The adsorption kinetics and isotherm could be expressed by pseudo-first-order and Langmuir equations, respectively. The comparison of the porosity and Hg adsorption of DRC and RC chlorinated residue obtained at 1000 °C, 10min indicated that Cl-adsorbed on the carbon in RC during chlorination may also be involved in Hg adsorption.

1. Introduction

Mercury is one of the most toxic heavy metals. When mercury is taken into the food chain, it accumulates in the animal's body and causes various organ malfunctions. Therefore, the allowable concentration of Hg in industrial wastewater is strictly regulated in Japan at 5 μg/L. In recent years, there has been a decrease in the number of cases of contamination in the greater water area, such as Minamata disease, but Hg contamination of the soil has become more apparent, and there are concerns about the accompanying contamination of groundwater and drinking water. Therefore, the development of technologies to remove Hg from wastewater and contaminated groundwater is an important issue.

Currently, coagulation-precipitation, ion-exchange and activated carbon adsorption methods are used for the treatment of industrial wastewater containing inorganic mercury. However, it is difficult to reduce the Hg concentration of the treated water below the effluent standard by coagulation-sedimentation treatment alone (Macchi et al., 1985). In addition, the ion-exchange and activated carbon adsorption methods have challenges in terms of equipment cost and regeneration cost (Deshkari et al., 1990). Recently, Hg performance with agricultural waste, biomass, coal, chitosan, and carbonaceous materials has been investigated as an alternative to these conventional methods (Xu et al., 2016; Li et al., 2017a; Vikrant and Kim, 2019; Hadi et al., 2015; Azimi et al., 2017; Dimpe and Nomngongo, 2017; Bailey et al., 1999; Xiao and Thomas, 2004; O'Connor et al., 2018; El-Shafey, 2010; Boutsika et al., 2014, 2017; Rocha et al., 2009, 2013; Krishnani et al., 2008; Song et al., 2013; Tan et al., 2016; Hai et al., 2013; Wajima and Sugawara, 2011; Yand et al., 2019; Velempini and Pillay, 2019; Miretxky and Cirelli, 2000). In these reports, $HgCl_2$(II) is mainly used as a mercury species. The morphology of mercury divalent in aqueous solutions depends on the pH of the solution, the co-halogen species and their concentration, and the dominant Hg species in acidic and neutral to basic solutions are HgCl, $HgCl^+$, Hg^{2+} and $Hg(OH)^2$(aq.), Hg(OH)(aq.), and it is also known that the Hg morphology varies with the pH of the medium (Knocke and Hemphill, 1982; Yoshida et al., 1976; Nishi et al., 1987). In the above report on Hg adsorption, the solution pH was studied in the acidic to neutral range (Xu et al., 2016; Li et al., 2017a; Vikrant and Kim, 2019; Hadi et al., 2015;

* Corresponding author.
E-mail address: tsubon@eng.hokudai.ac.jp (N. Tsubouchi).

https://doi.org/10.1016/j.jclepro.2021.127176
0959-6526/

Azimi et al., 2017; Dimpe and Nomngongo, 2017; Bailey et al., 1999), and for carbonaceous adsorbents (activated carbons/biochars) that have not been modified by hetero (O or S) or other means, it is thought that the oxygen-containing functional groups and charge states on the surface affect the adsorption performance (Xu et al., 2016; Li et al., 2017a; Vikrant and Kim, 2019; Hadi et al., 2015; Azimi et al., 2017; Dimpe and Nomngongo, 2017; Bailey et al., 1999; Xiao and Thomas, 2004; O'Connor et al., 2018; El-Shafey, 2010; Boutsika et al., 2014, 2017; Rocha et al., 2009, 2013; Krishnani et al., 2008; Song et al., 2013; Tan et al., 2016; Hai et al., 2013; Kai et al., 2001a, 2001b). However, in general, the adsorption capacity of Hg ions by biochar and activated carbon using the above oxygen-containing functional groups and different charge states is small.

We have investigated the production of $SiCl_4$ from rice husk char (RC) by the chlorination method as part of the development of effective utilization methods for rice husk, which is agricultural waste (Mochizuki et al., 2020). In this paper, we show that the Cl−Cl bond of Cl_2 gas is dissociated during the chlorination of RC and Cl atom is adsorbed on the carbon. It was also found that the chlorinated residue (Cl-loaded carbon) after the volatile separation of $SiCl_4$ from the rice husk char has a Hg ion adsorption performance. However, the details remain unclear.

Therefore, the main objective of this study was to elucidate in detail the Hg ion adsorption performance of Cl-loaded carbons obtained after chlorination of RC, firstly, chlorine content/morphology/porosity of Cl-loaded carbons prepared at different temperatures were investigated. Subsequently, the adsorption performance of Cl-loaded carbon prepared from RC and demineralized RC (DRC) was tested. The effect of Cl on Hg adsorption was then investigated by comparing the adsorption performance of Cl-loaded carbons prepared from RC and DRC.

2. Experimental

2.1. Sample

Rice husks (RH) in Japan were used as the sample. Samples were pyrolyzed at 800 °C in high-purity N_2 (99.999%) at 10 °C/min in a flow type fixed-bed quartz reactor to prepare chars (RCs). Samples were also used in which RC was de-mineralized by immersion in 48% HF solution at 108 °C for 12 h (Mochizuki et al., 2019). In this study, the char that was pyrolyzed at 800 °C and the char that was demineralized were referred to as RC and DRC, respectively. The analytical values of RH, RC, and DRC used are shown in Table 1. RC was crushed and sieved to −200 mesh and then subjected to chlorination experiments.

2.2. Chlorination

A flow-type fixed-bed quartz made reactor was used for the chlorination of RC or DRC (Mochizuki et al., 2020). The schematic diagram of experimental equipment listed at Fig. S1 in Supplemental Material. The temperature of the reactor was measured and controlled by inserting a thermocouple vertically from the outside of the furnace and making contact with the outer part of the reaction tube. For the experiment, 1.0 g of the sample was first weighed into an alumina boat, inserted into the center of the reaction tube, and then the sample was heated in Cl_2 (99.99%) at a heating rate of 20 °C/min, a maximum reaching temperature of 200−1000 °C, and a holding time of 0−60 min. The Cl_2 and volatile products were completely absorbed by a trap containing sodium hydroxide solution at the outlet of the reaction tube. After the target temperature or time was reached, the gas was switched to N_2 and the furnace was cooled to room temperature. The sample was then removed from the reactor and the yield of the solid sample was calculated by Eq. (1) by measuring its weight.

$$Y = W_i/W_0 \times 100 \quad (1)$$

Here, Y, W_i, and W_0 are yield (wt%), sample weight after chlorination (g), and sample weight before chlorination (g), respectively.

The ash content in the solid sample recovered after chlorination was determined from the post-combustion gravimetric measurement at 815 °C in accordance with JIS M8812. The volatility rate of ash during chlorination was calculated by the following Eq. (2).

$$R_{ash} = A_i/A_0 \times 100 \quad (2)$$

Here, R_{ash}, A_i, and A_0 mean release extent of ash (wt%), ash content in sample after chlorination (g) and ash content in sample before chlorination (g), respectively.

In this study, chlorination residue is indicated in terms of RC chlorination temperature. For example, the residues obtained by the 600 °C and 1000 °C, 10min holding during chlorination treatments are denoted as RC600 and RC1000_10, respectively.

2.3. Quantitative of ash composition and chloride

The dissolution of ash in the prepared samples was performed with a mixed acid of $HCl/HNO_3/HF$ as previously reported (Tsubouchi et al., 2014). The content of each element in the solution was measured by ICP-OES (Induction Plasma Optical Emission Spectrometry). The volatility of each element during chlorination was calculated by Eq. (3).

$$R_{element} = E_i/E_0 \times 100 \quad (3)$$

Here, $R_{element}$, E_i, and E_0 show release extent of element (%), element content in sample after chlorination (g), and elements content in sample before chlorination (g), respectively.

The chlorine content in the samples before and after chlorination was measured by ion chromatography with an automatic combustion device. The chlorine content of 0.1 g of the chlorinated sample treated with water in 100 mL of distilled water for 12 h was also analyzed by ion chromatography with an automatic combustion device in order to examine the form of chlorine present in the

Table 1
Composition of slag samples used in this study.

Sample	Elemental analysis, wt%-daf				Ash, wt%-dry	Ash composition, wt%-ash content basis								
	C	H	N	S + O[a]		Si	Ca	Mg	K	Na	P	Mn	Fe	Al
RH	46.9	5.9	0.53	46.7	20.4	9.1	0.11	0.05	0.28	0.02	0.08	0.03	0.01	0.01
RC	89.1	2.0	0.51	8.4	49.5	21.6	0.31	0.13	0.73	0.73	0.20	0.09	0.05	0.02
DRC	89.1	1.2	0.63	9.0	1.0	n.a.[b]								

[a] Estimated by difference.
[b] Not analyzed.

solid sample after chlorination and the chlorination reaction. The pore character of the sample was determined by the N_2 adsorption/desorption isotherms using the N_2 adsorption method, and then the BET and BJH methods were used to calculate the pore character (Brunauer et al., 1938; Barrett et al., 1951). The BET method is an analytical method that extends the Langmuir theory to the adsorption of multi-molecular layers of adsorbed gas molecules, and is the most common method for calculating the specific surface area. The specific surface area as can be calculated from the amount of adsorbed gas required to form a monolayer (unimolecular adsorption amount V_m) and the area occupied by the adsorbed gas molecules on the solid (molecular occupied cross section σ) (Eq. S1 in Supplemental material). V_m is calculated from the slope and intercept of the BET plot, where the relative pressure (P/P_0) is plotted on the horizontal axis and P/V_a (P_0−P) on the vertical axis, and the specific surface area is calculated (Eq. S2 in Supplemental material). The BJH method is based on Kelvin's capillary condensation theory and assumes that the mesopores are cylinders, and is widely used to analyze the pore distribution of mesopores. In that method, the pore diameter is obtained from the desorption isotherm, which is the relationship between the relative pressure and the amount of adsorbed material when the adsorbent desorbs.

2.4. Adsorption of Hg

The mercury adsorption of RC and chlorinated residue was investigated using 0.01−20 × 10^3 mg-Hg/L of $HgCl_2$ solution; 0.1 g of sample was added to 10 mL of mercury solution and stirred at 150 oscillation per min and 25 °C. The pH of the Hg solution used in this study was in the range of 2−2.5, and there was almost no significant change in pH before and after the experiment. 0.1 mL was sampled at any given time. The concentration of Hg in the solution was measured with a mercury analyzer. Mercury adsorption was calculated by Eq. (4).

$$q_e = \frac{V(C_0 - C_e)}{W} \quad (4)$$

where q_e is the amount of Hg ion adsorption at equilibrium (mg/g), C_0 and C_e are the initial and equilibrium Hg concentrations (mg/L), W is the adsorbent weight (g), and V is the volume of the solution (L).

3. Results and discussion

3.1. Volatile behavior of ash component during chlorination of RC

Fig. 1 shows the chlorinated residue yield and the volatile behavior of ash when RC is chlorinated. Yields increased above 300 °C and reached 110 wt% by 500−600 °C. On the other hand, increasing the chlorination temperature showed a decreasing trend in yield, which remained almost constant at 45 wt% at 1000 °C retention; ash in RC volatilized from above 400 °C, with a 75% volatility by 1000 °C; at 1000 °C retention, the volatility increased to 80% by 10min, but remained almost constant thereafter. Although ash volatilization occurs from above 400 °C as described above, an increase in yield was observed at 400−600 °C. In other words, the chlorinated residue yield increased despite the decrease in ash content. According to previous reports, Cl_2 gas readily dissociates on the carbon surface and the dissociated chlorine atoms adsorb on the carbon via C−Cl bonds (Amorebieta, 1985; Hu et al., 2014). Therefore, the increase in yield could be attributed to the adsorption of Cl on RC. (More on that later.)

Table 2 shows the volatility of the ash constituent elements corresponding to Fig. 1. The elements (Al, Fe, Mn) whose content in

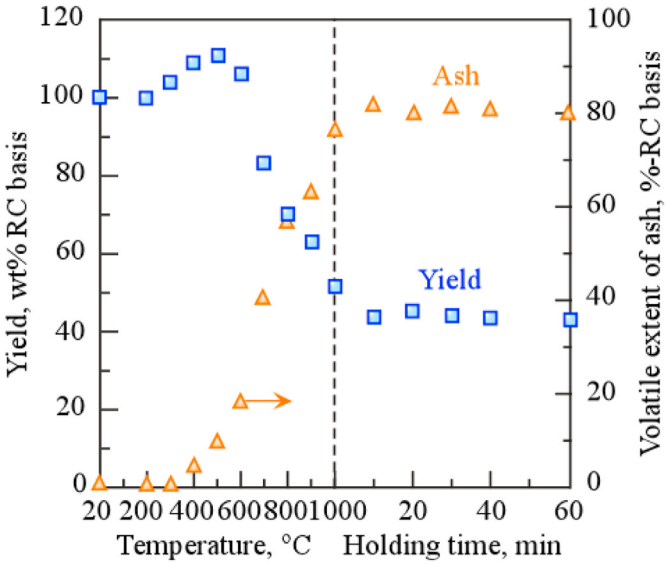

Fig. 1. Changes in yield of chlorination residue and volatile extent of ash during chlorination.

RC was less than 0.1% were excluded from this study. The volatilization of Si, the main component of the ash, was observed above 300 °C, and the volatilization extent up to 600 °C reached about 20%; at 600−700 °C, the volatilization of Si progressed rapidly and tended to increase with increasing temperature thereafter; at 1000 °C, the volatilization extent of Si was 75%. The volatile behavior of Si was almost consistent with that of ash. A similar volatile behavior was also observed in P. The volatilization of alkali metals (Na and K) occurred rapidly from above 800 °C, with 40−50% volatilization by 1000 °C; Mg volatilization was also observed from around 700-800 °C, but the volatilization extent by 1000 °C was small, less than 20%; Ca hardly volatilized by 1000 °C; Si and P volatilization increased by <10% by 10min of retention at 1000 °C, but did not increase thereafter. On the other hand, the volatility of Na and K increased significantly, reaching almost 100% by 10min of retention. The volatility of Mg and Ca for alkaline earth metals increased with increasing time up to 20−30min of retention time, but remained almost constant after 30min. The extent of the increase in volatility was greater for Mg. From these results, it was found that more than 80% of the ash (mainly Si) was desorbed during the chlorination of RC. In addition, it is concluded that release extent of element during chlorination depends on temperature. The volatile forms of each elements by thermodynamic equilibrium calculations using HSC Chemistry 5.1 (Outokumpu Research Oy.) were $SiCl_4$(g), PCl_3(g), NaCl(g), KCl(g), and $MgCl_2$(g); this calculation is based on the compositional values of each element in RC shown in Table 1 and the assumption that it exists as an oxide. The melting and boiling points of $SiCl_4$(g), PCl_3(g), NaCl(g), KCl(g), or $MgCl_2$(g) are −70 and 57, -112 and 76, 800 and 1465, 776 and 1420, or 714 and 1412 °C, respectively. Therefore, Si, P, Na, and K may volatile as $SiCl_4$(g), PCl_3(g), NaCl(g), and KCl(g) during chlorination of RC, due to low melting and boiling points. On the other hand, the low volatility of Mg and Ca may be due to the high melting and boiling points of these chloride species.

3.2. Characterization of chlorinated residue

Table 3 shows the results of the investigation of the pore character of the chlorinated residues. The surface area of the RC was very small, <10 m^2/g or less, whereas its value increased with

Table 2
Summaries of volatile extent of element in RC during chlorination.

Chlorination temperature, °C	Volatile extent of element, %						Holding time at 1000 °C, min	Volatile extent of element, %					
	Si	Ca	Mg	K	Na	P		Si	Ca	Mg	K	Na	P
400	5	0	0	0	0	0	0	75	0	10	49	60	69
500	10	0	0	1	1	5	10	84	4	28	99	97	75
600	25	0	0	1	17	14	20	83	8	29	100	98	75
700	50	0	0	1	36	43	30	82	9	33	100	99	76
800	62	0	0	3	45	53	40	82	10	33	100	99	76
900	68	0	3	17	57	60	60	83	11	32	100	99	75
1000	75	0	10	49	60	67	–	–	–	–	–	–	–

Table 3
Summarizes of yield of chlorinated residue, volatile extent of ash, and pore structure.

Chlorination temperature, °C	Yield of chlorinated residue, wt%	Volatile extent of ash, %	Pore structure		Holding time at 1000 °C, min	Yield of chlorinated residue, wt%	Volatile extent of ash, %	Pore structure	
			S_{BET}[a] m^2/g	Pore volume[b] cm^3/g				S_{BET}[a] m^2/g	Pore volume[b] cm^3/g
400	109	5	<10	0.01	0	52	75	315	0.18
500	111	9	10	0.02	10	44	80	335	0.18
600	106	19	40	0.03	20	45	80	330	0.18
700	83	45	155	0.10	30	45	80	n.a.[c]	n.a.[c]
800	70	57	195	0.19	40	44	80	n.a.[c]	n.a.[c]
900	63	63	245	0.19	60	44	80	n.a.[c]	n.a.[c]
1000	52	75	315	0.18	–	–	–	–	–

[a] Calculated by three points Brunauer Emmett Teller method.
[b] Calculated by Barrett Joyner Halenda method.
[c] Not analyzed.

increasing chlorination temperature to 40 m^2/g at 600 °C. A rapid increase in surface area was observed at 600–700 °C, where ash volatilization progressed, and the surface area increased linearly at 700–1000 °C, reaching 315 m^2/g at 1000 °C. On the other hand, there was almost no change in surface area at 1000 °C retention, where ash volatilization was almost unobserved. A similar trend was observed for the pore volume. The relationship between ash volatility rate and surface area and pore volume was investigated, and a relatively good positive correlation was found between ash volatility extent and surface area. The pore size distribution was examined by BJH method from the observed N_2 adsorption/desorption isotherms, and the pore peaks around 4 nm observed in RC increased with the chlorination temperature. These results indicate that SiO_2 in RC is mainly present in the carbon matrix on the order of a few nm, and that their volatilization during chlorination led to the development of mesopores in the residue (see Fig. 4 below). It is also thought that the rate of ash (mainly Si) chloride volatilization decreased due to the development of pores due to Si volatilization at >700 °C during chlorination and the rate-controlled diffusion of chlorine gas into the carbon pores.

In order to investigate whether Cl_2 gas dissociates on the RC and adsorbs on the RC surface, we investigated the change in yield and chlorine content when RC and DRC were chlorinated, and the results are shown in Fig. 2. As mentioned above, the yield of RC increased to 600 °C and then decreased to 1000 °C and remained almost constant thereafter; the yield of DRC also increased from 300 to 600 °C and reached 140 wt%. On the other hand, the yield decreased from 600 to 1000 °C and remained almost constant (100 wt%) above 10min at 1000 °C. The behavior of this increase or decrease in yield was similar to that of RC. As shown in Table 1, the ash content in the DRC decreased by 1.0 wt%-dry. The Cl content in RC and DRC increased rapidly (22–35%) by 600 °C, as shown in Fig. 2a, and then decreased significantly (10%) as the temperature increased to 1000 °C. The value was almost constant at 1000 °C. Therefore, it can be concluded that the increase in yield is due to the adsorption of Cl on the DRC. On the other hand, the yield decreased above 600 °C, suggesting that the Cl species adsorbed on the carbon desorb with increasing temperature. Interestingly, the amount of Cl adsorbed on the DRC by 600 °C (35%) was greater than the RC (25%). This can be attributed to the removal of ash from the DRC by HF treatment and the porosity of the carbonaceous material, as shown in Table 1. In other words, it can be said that the removal of SiO_2 beforehand made it porous, making it easier for the chlorine gas to access the carbon active site and increasing the amount of adsorbed Cl. These results indicate that Cl_2 gas dissociates on the carbons in RC and DRC by 600 °C to form C–Cl bonds, which are subsequently desorbed by increasing temperature.

In RC and DRC, the yields of chlorinated residues tended to decrease with water treatment regardless of the chlorination temperature (Fig. 3a, c). In RC, both H_2O-soluble and insoluble Cl increased by 600 °C (Fig. 3b), but the ratio was larger in the latter, while both H_2O-soluble and insoluble Cl decreased from 600 to 1000 °C. On the other hand, in DRC, most of the Cl in the solid phase was water insoluble regardless of the chlorination temperature (Fig. 3d), and more H_2O-soluble Cl species were found in RC than in DRC. $SiCl_4$, an Si chloride that represents the majority of the ash, is likely to volatilize quickly after chlorination in terms of its melting point (−70 °C)/boiling point (50 °C). Even if it remains in the solid phase as $SiCl_4$ due to diffusion in the solid, the species hydrolyzes with water and precipitates as SiO_2. Therefore, it is possible that the Cl species derived from $SiCl_4$ remaining in the solid phase was detected as water-soluble fraction Cl. On the other hand, the pore characteristics of RC and DRC are significantly different and the amount of active sites is thought to be different, and in the former, the volatilization of ash constituent elements during the chlorination treatment results in the development of pores and the formation of active sites in the *in-situ*, which may also react with Cl_2 gas (Amorebieta, 1985; Hu et al., 2014; Tsubouchi et al., 2016). This may be the reason why there are so many water-soluble Cl species in RC. A detailed study is a matter for the future.

Table 4 and Fig. 4 show the changes in the pore structure of chlorinated RC before and after H_2O treatment; up to RC500, there

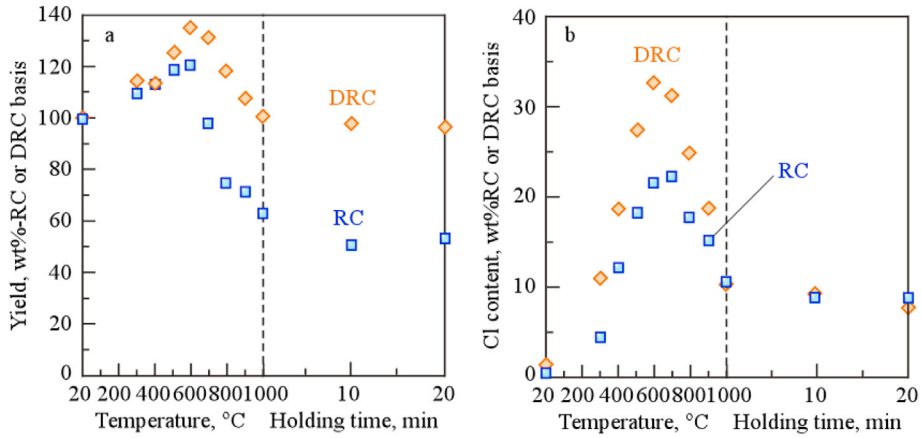

Fig. 2. Changes in yield of RC or DRC (a) and Cl content (b) during chlorination of RC and DRC.

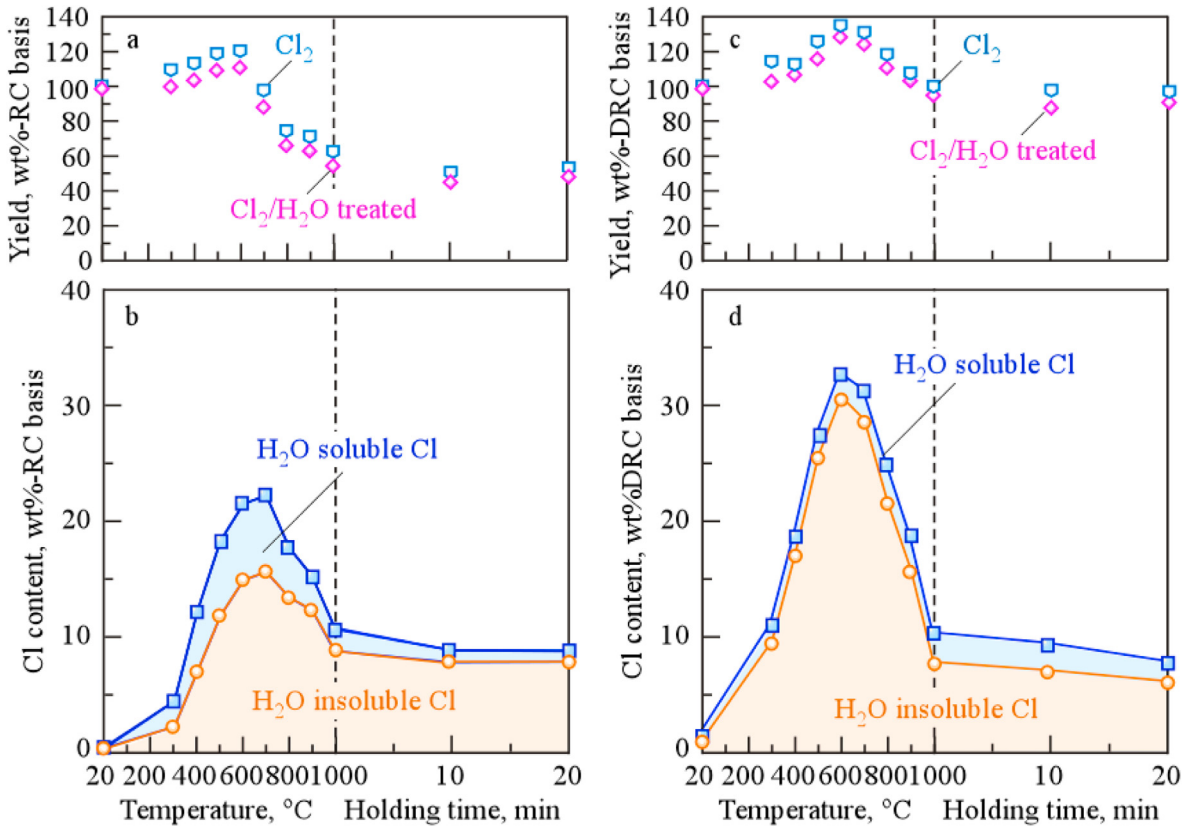

Fig. 3. Changes in yield (a, c) and H_2O soluble-/insoluble-Cl (b, d) before and after H_2O treatment of chlorinated RC (a, b) or DRC (c, d).

was almost no change in surface area and pore volume before and after water treatment; however, RC600 with high Cl content showed a remarkable development of pore structure after water treatment (Fig. 4a). This is thought to be due to the leaching of H_2O-soluble Cl adsorbed on the carbon into the water by water treatment. On the other hand, the surface area and pore volume of the H_2O-treated samples of DRC600 and DRC1000_10, which have the maximum Cl content and constant Cl content, respectively, were 245 m^2/g and 0.23 cm^3/g and 570 m^2/g and 0.27 cm^3/g, respectively. These values tended to be larger than those of chlorinated DRC600 (225 m^2/g, 0.23 cm^3/g) and DRC1000_10 (545 m^2/g, 0.28 cm^3/g), suggesting that pores developed in DRC due to the elution of water-soluble Cl by water treatment. This is supported by the increase in the pore size peak of DRC600 after water treatment compared to before water treatment as shown in Fig. 4b. These results indicate that the Cl species formed on the carbon by dissociation of Cl_2 gas on the carbon, most of which are insoluble in water, affect the change in the porosity.

3.3. Kinetic of mercury adsorption by chlorinated residue of RC

Fig. 5a shows the change in the amount of adsorption over time when chlorinated residues (RC, RC300, RC500, RC700, RC900, and RC1000_10) obtained at each temperature were subjected to Hg adsorption experiments in a 4.8×10^3 mg-Hg/L solution. For both chlorinated residues, the amount of Hg adsorption increased by 8 h

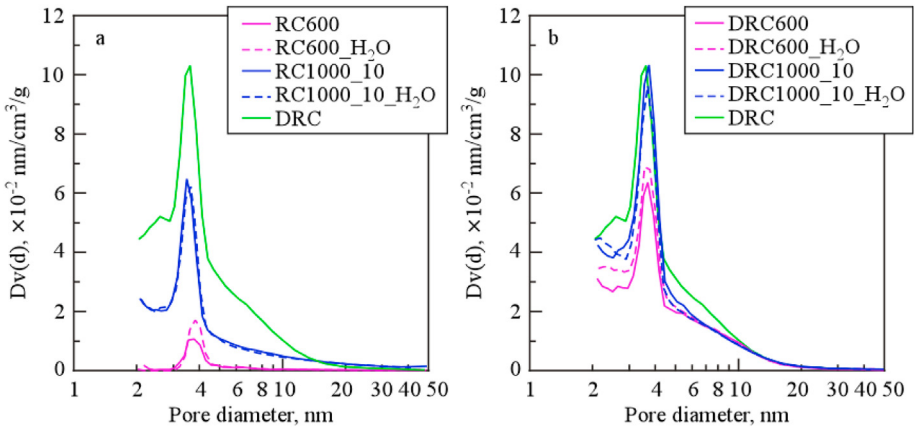

Fig. 4. Pore size distribution of before and after H_2O treatment of chlorinated RC (c) or DRC (b).

Table 4
Summarizes of pore structure and Cl content of chlorinated residue before and after H_2O treatment.

Sample	Before H_2O treatment			After H_2O treatment		
	Pore structure		Total-Cl	Pore structure		Total-Cl
	S_{BET}, m^2/g[a]	Pore volume, cm^3/g[b]		S_{BET}, m^2/g[a]	Pore volume, cm^3/g[b]	
RC	<10	<0.01	0.5	<10	<0.01	0.5
RC300	<10	<0.01	5	<10	<0.01	2
RC400	<10	<0.01	12	10	0.02	7
RC500	10	0.02	18	10	0.02	12
RC600	40	0.03	22	55	0.03	15
RC700	155	0.10	22	210	0.13	16
RC800	195	0.19	18	270	0.23	14
RC900	245	0.19	15	320	0.22	12
RC1000	315	0.18	11	325	0.17	9
RC1000_10	335	0.18	9	340	0.19	8
DRC	405	0.33	0.3	n.a.	n.a.	n.a.
DRC600	225	0.23	30	245	0.23	2
DRC1000_10	545	0.28	7	570	0.27	2

c Not analyzed.
[a] Calculated by three points Brunauer Emmett Teller method.
[b] Calculated by Barrett Joyner Halenda method.

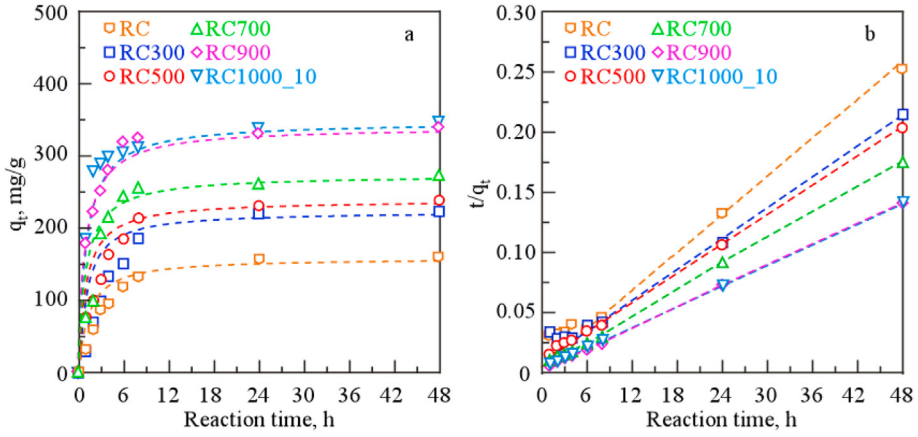

Fig. 5. Mercury adsorption of RC and chlorinated RC as a fraction of reaction time (a) and plot of t/q_t and reaction time (b).

and remained almost constant thereafter. The pecking order for the amount of adsorption at 48 h was RC < RC300 < RC500 < RC700 < RC900 < RC1000_10, which tended to increase with increasing chlorination temperature. The rate constants k_1 and k_2 were obtained from the analysis by Lagergen's pseudo-first-order (Eq. (5)) and pseudo-second-order (Eq. (6)) equations based on the relationship of the amount of adsorption to the reaction time.

$$\ln(q_e - q_t) = \ln q_e - k_1 t \quad (\text{Pseudo} - \text{first} - \text{order}) \tag{5}$$

$$\frac{t}{q_t} = \frac{1}{k_2 q_e^2} + \frac{t}{q_e} \quad (\text{Pseudo} - \text{second} - \text{order}) \tag{6}$$

where q_e is the adsorption capacity (equilibrium adsorption) (mg/g), q_t is the Hg ion adsorption at time t (mg/g), k_1 is the pseudo-primary reaction rate constant (1/h), and k_2 is the pseudo-secondary reaction rate constant (g/mg· h). The respective reaction rate constants k_1 and k_2 were obtained from the slope of the linear relationship between $ln(q_e\text{-}q_t)$ and t/q_t values with respect to reaction time T in the pseudo-first and pseudo-second order reaction rate equations, respectively. The results are summarized as kinetic parameters in Table 5, and the relationship between reaction time and t/qt is shown in Fig. 5b. Using the pseudo-first-order reaction rate equation, k_1 and correlation coefficient R^2 were in the range of 0.1168–0.258 1/h and 0.673–0.992, respectively, and both tended to decrease as the chlorination temperature increased. On the other hand, when the pseudo-second order rate equation was used, a relatively good linear relationship was found between the reaction time t and t/q_t, as shown in Fig. 5b, and the reaction rate constant k_2, which was determined from the slope, was in the range of 0.0028–0.005 g/mg· h. The correlation coefficients were >0.997 for all the chlorinated residues. These correlation coefficients were higher than those of the pseudo-first-order reaction model. By fitting the experimental data with the pseudo-secondary reaction rate constant k_2 obtained above, it is clear that the experimental data can be fitted relatively well as shown by the dashed line in Fig. 5a. If the Cl species supported on the RC during chlorination were involved in the adsorption of Hg ions, high adsorption performance should be observed in RC500-700 with a large Cl content as shown in Fig. 3b, but the degree of adsorption was smaller than that of RC1000_10. This consideration is discussed below.

Fig. 6a shows the relationship between the amount of adsorption and the chlorination temperature at the reaction rate constant k_2, $t = 48$ h, obtained from the pseudo-secondary rate analysis. The reaction rate constant k_2 decreased almost linearly with increasing chlorination temperature, and a negative correlation between the two was found ($R^2 = 0.9678$). In contrast, the adsorption capacity q_e increased linearly with increasing chlorination temperature ($R^2 = 0.9516$). These results suggest that the chlorination temperature is an important factor in the Hg adsorption capacity of RC chlorinated residues. Next, the relationship between the surface area of the RC chlorinated residue shown in Table 3 and the adsorption capacity at $t = 48$ h is plotted in Fig. 6b. A positive correlation between the adsorption capacity and surface area was found (except for RC), although there was some variability. There was also a positive correlation between the adsorption capacity and the pore volume, but the degree of correlation was greater for the surface area. On the other hand, there was no clear correlation between the amount of Hg adsorption and the amount of total chlorine content, water soluble and insoluble Cl in the RC chlorinated residue shown in Table 4. As mentioned above, the reason for the smaller Hg adsorption of RC500-700 with higher Cl loading compared to RC1000_10 may be due to the smaller surface area of 10–155 m^2/g in the former and 335 m^2/g in the latter. As is well known, the adsorption capacity of Hg on activated carbon depends on the porosity of the activated carbon used (Kadota, 1993). Therefore, the pore size of RC may have an important influence on the adsorption performance of Hg by RC chlorinated residues.

Table 5
Kinetic parameter of the result of Fig. 5

Sample	Pseudo-first order		Pseudo-second order	
	k_1, 1/h	R^2	k_2, g/mg· h	R^2
RC	0.1674	0.985	0.0050	0.999
RC300	0.1818	0.992	0.0045	0.999
RC400	0.1522	0.965	0.0043	0.999
RC500	0.1387	0.896	0.0042	0.999
RC600	0.1168	0.774	0.0040	0.999
RC700	0.1216	0.682	0.0037	0.997
RC800	0.1202	0.707	0.0034	0.999
RC900	0.1358	0.673	0.0030	0.999
RC1000	0.1431	0.826	0.0028	0.999
RC1000_10	0.2528	0.741	0.0029	0.999

3.4. Kinetic of mercury adsorption by chlorinated residue of DRC

In order to investigate whether the Cl species adsorbed on RC during chlorination affects the Hg adsorption, the Hg adsorption performance of the residue obtained by chlorination of DRC was investigated. The sample used was DRC with almost no Cl, and the DRC chlorinated residue was DRC600, which had the largest amount of Cl in Fig. 3, and DRC1000_10, which had completed the desorption of Cl. As shown in Fig. 7a, the adsorption volume of RC, DRC, chlorinated RC, and DRC in 4.8 × 10^3mg-Hg/L solution was increased by 8 h and remained constant thereafter. The order of adsorption volume at 48 h was DRC600 < RC ≪ AC < DRC < RC1000_10 < DRC1000_10. The adsorption volume at $t = 48$ h observed for DR1000_10 was greater than that for sulfur-loaded carbon (El-Shafey, 2010; Wajima and Sugawara, 2011), indicating that this adsorbent has excellent performance. Based on the adsorption data in Fig. 7a, the rate analysis factors for the pseudo-first- and pseudo-second-order reaction rate equations are summarized in Table 6, and the relationship between reaction time and t/q_t is shown in Fig. 7b. In the pseudo-primary reaction rate model, k_1 and correlation coefficient R^2 were in the range of 0.0995–0.1674 1/h and 0.6267–0.985, respectively, and the correlation coefficients were small. On the other hand, when the pseudo-secondary reaction rate model was used, a relatively good linear relationship between reaction time t and t/qt was observed as shown in Fig. 7b, and the reaction rate constant k_2 calculated from the slope was in the range of 0.0028–0.0079 g/mg· h. The correlation coefficients were >0.983 for all the samples. The experimental data were fitted using the pseudo-secondary reaction rate constant k_2 obtained above, and the data were represented relatively well as shown by the dashed line in Fig. 7a.

3.5. Equilibrium adsorption of mercury by RC, DRC, and chlorinated samples

The results of the adsorption equilibrium study using $HgCl_2$ solution with Hg concentration of 0.01–20 × 10^3 mg/L-Hg are shown in Fig. 8a. In all samples, Hg adsorption tended to increase to Hg concentrations up to 10 × 10^3 mg/L and remained almost constant above that level. The adsorption curves obtained at varying initial Hg concentrations were analyzed using Langmuir (Eq. (7)) and Freundlich (Eq. (8)) adsorption isotherms.

$$q_e = \frac{q_m K_L C_e}{1 + K_L C_e} \quad (\text{Langmuir}) \tag{7}$$

$$q_e = K_F C_e^{1/n} \quad (\text{Freundlich}) \tag{8}$$

where, q_m is the equilibrium adsorption amount (mg/g), K_L and K_F are the Langmuir (L/mg) and Freundlich constant, respectively. In the Langmuir analysis, the relationship between equilibrium

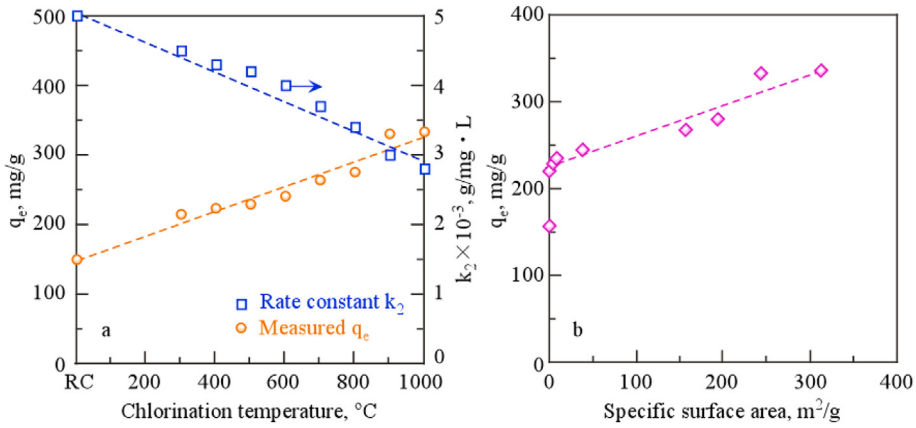

Fig. 6. Relation between chlorination temperature and rate constant or mercury adsorption amount at 48 h used 4.8 × 10^3mg-Hg/L solution (a) and relationship between mercury adsorption amount at 48 h used 4.8 × 10^3mg-Hg/L solution and specific surface area (b).

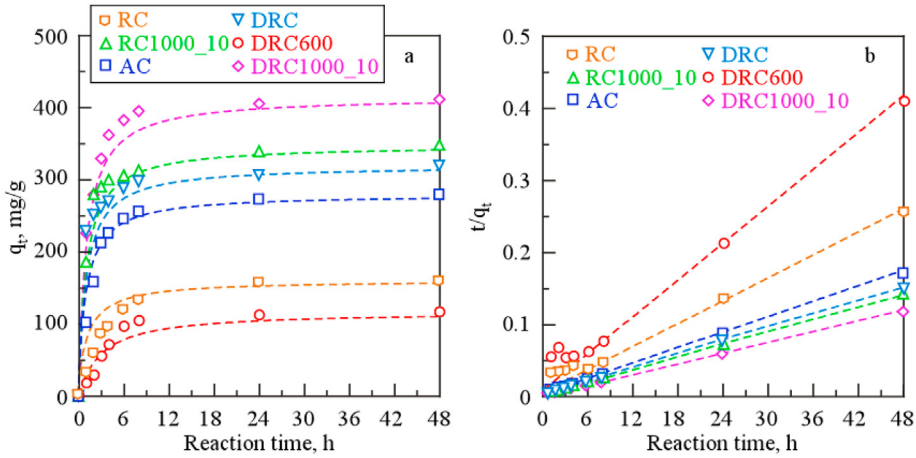

Fig. 7. Mercury adsorption of RC, chlorinated RC, DRC, and chlorinated DRC as a fraction of reaction time (a) and plot of t/q_t and reaction time (b).

Table 6
Kinetic parameter of the result of Fig. 7

Sample	Pseudo-first order		Pseudo-second order	
	k_1, 1/h	R^2	k_2, g/mg· h	R^2
RC	0.1674	0.985	0.0050	0.999
RC1000_10	0.1431	0.826	0.0028	0.999
DRC	0.0995	0.627	0.0031	0.999
DRC600	0.1384	0.844	0.0079	0.983
DRC1000_10	0.1359	0.690	0.0024	0.999
AC	0.1408	0.825	0.0036	0.999

concentration C_e and C_e/q_e values was plotted, and the saturated adsorption and Langmuir constants were obtained from the slope and intercept of the obtained linear relationship, respectively; in the Freundlich analysis, *log* q_e values were plotted against log C_e (Fig. 8b), and the adsorption rate constants ($1/n$) and Freundlich constants were obtained from the slope and intercept of the obtained linear relationship. The results are summarized in Table 7.

The Freundlich adsorption rate constant and constant K_F calculated from the adsorption capacity shown in Fig. 8a were in the range of 0.625–0.850 and 0.231–0.657, respectively. Although these parameters were used to fit the results of this experiment with the Freundlich equation, they did not represent the experimental results well. On the other hand, in the Langmuir analysis, the K_L was in the range of 0.199–0.884 L/mg, and the experimental results were fitted using this Langmuir constant with relatively good accuracy as shown by the dashed line in Fig. 8a. The maximum adsorption capacities q_m of RC, RC1000_10 DRC, DRC600, DRC1000_10, and AC calculated from the Langmuir equation were 216, 617, 647, 198, 884, and 540 mg/g, respectively. The order of the maximum adsorption volume was DRC600 < RC ≪ AC < RC1000_10 < DRC < DRC1000_10. When 4.8 × 10^3mg-Hg/g of $HgCl_2$ solution was used, the order of the adsorption volume at 48 h of the chlorinated residue was consistent with the order of chlorination temperature and surface area, but no relationship with surface area was found in the present study. Interestingly, of the samples used, the surface area of AC was the largest at 1500 m^2/g, but the maximum adsorption capacity was the largest at DRC1000_10 with a surface area 1/3 of AC (545 m^2/g).

Table 7 also shows the results of calculating the Hg adsorption per surface area of each sample, assuming a surface area of 10 m^2/g since the surface area of RC was less than 10 m^2/g. The pecking order of Hg adsorption capacity per surface area (excluding RC) was AC < DRC600 < DRC = DRC1000_10 < RC1000_10, which was different from the pecking order of maximum adsorption capacity. The results indicate that the chlorinated residue has a high Hg adsorption performance.

As shown above, it is difficult to determine the effect of chlorine only from the measured adsorption performance because the porosity of RC and DRC is changed by the desorption of ash and the

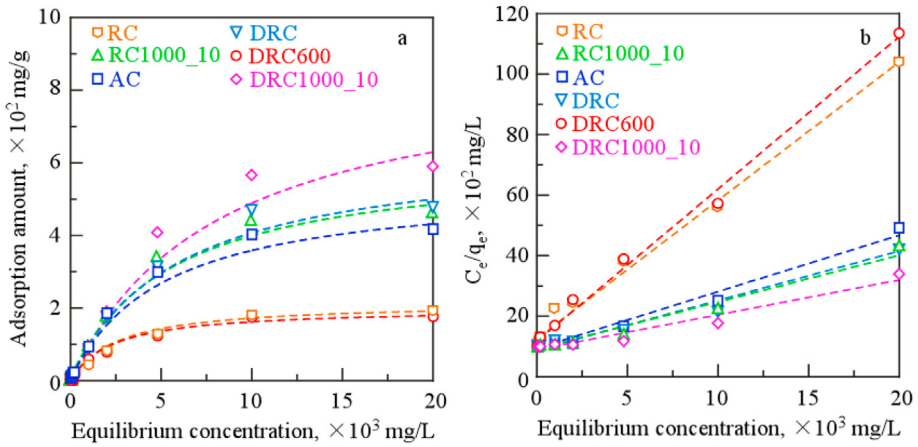

Fig. 8. Equilibrium adsorption of mercury by RC, DRC, and chlorinated samples (a) and plot of C_e/q_e and equilibrium concentration (b).

Table 7
Parameter of the result of Fig. 8

Sample	Freundlich			Langmuir			S_{BET} m^2/g[a]	q_m/S_{BET} mg-Hg/m^2
	1/n	K_F	R^2	q_m, mg-Hg/g	K_L, L/mg	R^2		
RC	0.625	0.267	0.984	216	0.217	0.990	<10	2.16
RC1000_10	0.809	0.577	0.971	617	0.617	0.975	335	1.90
DRC	0.808	0.580	0.977	647	0.647	0.978	405	1.62
DRC600	0.617	0.231	0.969	198	0.199	0.994	225	0.81
DRC1000_10	0.850	0.657	0.978	884	0.884	0.954	545	1.62
AC	0.793	0.556	0.966	540	0.540	0.974	1500	0.36

[a] The value before H_2O-treatment.

adsorption of chlorine on carbon in the chlorination process. Most of the SiO_2 in the RC is removed by HF treatment and becomes porous. In other words, the increase in surface area in DRC can be considered to be due to the removal of SiO_2 and other ashes. Then, first of all, the maximum Hg adsorption amount per m^2 is calculated from the difference between the surface area of RC and DRC (10, 405 m^2/g) and the maximum adsorption capacity (216, 647 mg/g) (denoted as ΔS_{BET}, Δq_m), and it becomes ΔS_{BET} = 390 m^2/g, Δq_m = 431 mg-Hg/g, $\Delta q_m/\Delta S_{BET}$ = 1.105 mg-Hg/m^2. Since the surface area of RC1000_10 is 335 m^2/g, the Hg adsorption amount corresponding to the increase in surface area of Si-derived desorbed by RC chlorination is calculated as 335 m^2/g × 1.105 mg/m^2 = 370 mg/g. However, the actual maximum Hg adsorption capacity of RC1000_10 is 617 mg-Hg/g. In other words, 265 mg-Hg/g (about 43%) of Hg on RC1000_10 is adsorbed to non-porous sites. It is thought that this corresponds to the Cl adsorbed on the carbon during the chlorination process.

As is well known, the form of mercury divalent in aqueous solutions depends on the pH of the solution, the coexisting halogen ion species and their concentrations, and the predominant Hg species in acidic solutions of $HgCl_2$(II) are $HgCl_2$, $HgCl^+$, and Hg^{2+} (Knocke and Hemphill, 1982; Yoshida et al., 1976; Nishi et al., 1987). Based on the amount of Cl in the H_2O insoluble fraction of RC1000_10 (8.9%) shown in Table 4, 496 mg-Hg is the amount of Hg that can be adsorbed on the Cl adsorption site, assuming that Hg and Cl adsorption occurs with $HgCl^+$ and C(Cl)–$HgCl^+$ in solution (where C(Cl) indicates the active site bound with C–Cl in RC). However, the actual amount adsorbed to the Cl adsorption site is 265 mg-Hg, and the rate of Hg adsorption to the Cl adsorption site on RC1000_10 is estimated to be 43%. On the other hand, if we assume that the Hg morphology to be adsorbed is Hg^{2+} in the form of 2C(Cl)–Hg^{2+}, 245 mg-Hg can be adsorbed, and this calculated value is almost consistent with the amount of Hg adsorbed on Cl adsorption sites other than the C site (265 mg-Hg) obtained above. Therefore, the main Hg adsorption form to the Cl site in RC1000_10 is considered to be 2C(Cl)–Hg^{2+}. According to previous studies investigating the Hg adsorption performance of biochar, it has been reported that biochar with high S content adsorbs Hg by Hg–S binding, whereas the main binding species of Hg in biochar with low S content are O and Cl (Liu et al., 2016; Li et al., 2017b; Gibson et al., 2011). According to a report by S XANES and Hg EXAFS that examined the Hg morphology adsorbed on the biochar, Cl in the biochar is thought to adsorb Hg ions with -Cl-Hg-Cl- (Liu et al., 2016; Li et al., 2017b; Gibson et al., 2011). Such a report supports the results of this study. It has also been reported that the adsorption site of Hg in the biochar is induced by π-electrons of C=C and C=O in addition to OH and COOH groups to induce Hg-π bonding (Liu et al., 2016; Li et al., 2017b; Gibson et al., 2011). Therefore, in addition to the adsorption on Cl and pores, π-electrons in the carbon structure may also act on Hg adsorption in Cl-loaded carbon. As is well known, FT-IR analysis of the adsorbent before and after the adsorption experiment may help to clarify the chemisorption properties. The results of FT-IR analysis of the adsorbent before and after the adsorption experiment are shown in Fig. S2 in supplemental material, but no clear difference was observed. Morphological analysis of Hg adsorption will be an important issue in the future.

RC600 and DRC600 showed a decrease in Hg adsorption despite the high Cl adsorption (Table 6 and Fig. 8a). The reason for this is currently unknown. However, as shown in Fig. 3, RC600 has a large amount of H_2O soluble Cl, and the Hg morphology in the Hg solution may have changed depending on the Cl species eluted, which may be one of the reasons for the decrease in adsorption capacity. However, in DRC600, the amount of H_2O soluble Cl is small and the amount of Cl eluted during the adsorption experiment is also small, but the adsorption capacity is decreased. Therefore, it can be said

that the elution of Cl species does not affect the Hg adsorption performance much under these conditions. More detailed investigation of the pore structure on the Hg adsorption performance is also an issue to be addressed in the future.

Finally, Comparison of chlorinated residue prepared in this work and the previous studies on Hg adsorbent performance from agricultural residues (El-Shafey, 2010; Krishnani et al., 2008; Song et al., 2013; Tan et al., 2016; Hai et al., 2013; Khalid et al., 1999; Inbaraj et al., 2009; Mishra and Chaudhury, 1996; Krishnan and Anirudhan, 2002; Cox et al., 1999) was made. The Hg adsorption performance (617 mg/g) of RC chlorinated residue prepared at 1000 °C, 10min was found to be higher than other agricultural residues (3.2–208 mg/g) (Mochizuki et al., 2020). In addition, the chlorinated residue of RC gave high Hg adsorption amount comparing with other sulfur-loaded carbon (217–526 mg/g). Therefore, this method is an environmentally friendly co-production of useful resources and environmental cleanup agents, because the residue produced when silica is recovered from rice husks is used as a mercury adsorbent.

4. Conclusions

This study was first investigated chlorine content/morphology/porosity of Cl-loaded carbons prepared by chlorination of rice husk char (RC) or demineralized RC (DRC) at different temperatures. The Cl content during chlorination of RC and DRC increased with increasing treatment temperature, reached a maximum value at 600 °C, and then decreased significantly by 1000 °C. Most of the Cl adsorbed on RC and DRC during the chlorination process was H_2O insoluble Cl. The pore morphology of the chlorinated residue of RC increased with increasing chlorination temperature; the pore morphology at 600 °C, where the Cl content was highest, was smaller than that of the sample treated at 1000 °C, indicating pore blockage due to adsorbed Cl. Then, the Hg adsorption performance of chlorinated residue of RC was examined. Hg adsorption performance of the chlorinated residues of RC prepared at each temperature increased with increasing chlorination temperature. The maximum Hg adsorption capacity of the chlorinated residue of RC obtained at 1000 °C and 10 min retention reached 620 mg/g, which is greater than that of commercial activated carbon. A positive correlation between the surface area of the RC chlorinated residue and the amount of Hg adsorbed was found, indicating the influence of the surface area on the adsorption performance. Subsequently, the effect of Cl on Hg adsorption was investigated by comparing the adsorption performance of Cl-loaded carbons prepared from RC and DRC. The Hg adsorption performance of the chlorinated residue treated with DRC at 1000 °C for 10min was greater than that of DRC or DRC chlorinated at 600 °C with a high Cl content. Comparison of the pore size and the amount of Hg adsorption of the chlorinated residue obtained by holding DRC at 1000 °C for 10min indicated that Cl adsorbed on the carbon in RC during chlorination may also be involved in the adsorption of Hg ions.

Declaration of competing interest

The authors declare that they have no known competing financial interests or personal relationships that could have appeared to influence the work reported in this paper.

Acknowledgments

This study was supported in part by a Grant-in-Aid for Challenging Research (Exploratory) from the Ministry of Education, Culture, Sports, Science and Technology, Japan, and by the Steel Foundation for Environmental Protection Technology (SEPT).

Appendix A. Supplementary data

Supplementary data to this article can be found online at https://doi.org/10.1016/j.jclepro.2021.127176.

Novelty statement

Mercury is one of the most toxic heavy metals. When mercury is taken into the food chain, it accumulates in the animal's body and causes various organ malfunctions. Therefore, the allowable concentration of Hg in industrial wastewater is strictly regulated. However, in general, the adsorption capacity of Hg ions by biochar and activated carbon using the above oxygen-containing functional groups and different charge states is small. The present study provides quantitative data relating mercury adsorbent with high adsorption ability prepared from chlorination of rice husk char. It may help to development of the purification of low cost waste water process.

References

Amorebieta, V.T., 1985. Direct study of the catalytic decomposition of chlorine and chloromethanes over carbon films. Int. J. Chem. Kinet. 17, 849.
Azimi, A., Azari, A., Rezakazemi, M., Ansarpour, M., 2017. Removal of heavy metals from industrial wastewaters: a review. ChemBio Eng. Rev. 4, 37–59.
Bailey, S.E., Olin, T.J., Bricka, R.M., Adrian, D.D., 1999. A review of potentially low-cost sorbents for heavy metals. Water Res. 33, 2469–2479.
Barrett, E.P., Joyner, L.G., Halenda, P.H., 1951. The determination of pore volume and area distributions in porous substances. I. Computations from nitrogen isotherms. J. Am. Chem. Soc. 73, 373–380.
Boutsika, L.G., Karapanagioti, H.K., Manariotis, I.D., 2014. Aqueous mercury sorption by biochar from malt spent rootles. Water Air Soil Pollut. 225, 1805.
Boutsika, L.G., Karapanagioti, H.K., Manariotis, I.D., 2017. Effect of chloride and nitrate salts on Hg(II) sorption by raw and pyrolyzed malt spent rootlets. J. Chem. Technol. Biotechnol. 92, 1912–1918.
Brunauer, S., Emmett, P.H., Teller, E., 1938. Adsorption of gases in multimolecular layers. J. Am. Chem. Soc. 60, 309–319.
Cox, M., Shafey, E.-E., Pichugin, A.A., Appleton, Q., 1999. Removal of Hg(II) from aqueous solution on a carbonaceous sorbent prepared from flax shive. J. Chem. Technol. Biotechnol. 75, 1019–1029.
Deshkari, A.M., Bokade, S.S., Daral, S.S., 1990. Modified hardwickia binate bark for adsorption of mercury(II) from water. Water Res. 24, 1011–1016.
Dimpe, K.M., Nomngongo, P.N., 2017. A review on the efficacy of the application of myriad carbonaceous materials for the removal of toxic trace elements in the environmental. Trends Environ. Anal. Chem. 16, 24–31.
El-Shafey, E.I., 2010. Removal of Zn(II) and Hg(II) from aqueous solution on a carbonaceous sorbent chemically prepared from rice husk. J. Hazard Mater. 175, 319–327.
Gibson, B.D., Ptacek, C.J., Lindsay, M.B.J., Blowes, D.W., 2011. Examining Mechanisms of groundwater Hg(II) treatment by reactive materials: an EXAFS study. Environ. Sci. Technol. 45, 1015–10421.
Hadi, P., To, M.-H., Hui, ChW., Lin, C.S.K., Mackay, G., 2015. Aqueous mercury adsorption by activated carbon. Water Res. 73, 37–55.
Hai, N.T.T., Hue, N.T., Trung, D.Q., 2013. Adsorption of Hg(II) from aqueous solution of activated carbon impregnated in copper chloride solution. Asian J. Chem. 25, 10251–10254.
Hu, M., Song, M., Lv, X., Liu, L., Bai, C., 2014. Carbo-chlorination of silica: thermodynamic simulation and experimental study. Asian J. Chem. 26 (11), 3227–3232.
Inbaraj, B.S., Wang, J.S., Lu, J.F., Siao, F.Y., Chen, B.H., 2009. Adsorption of toxic Hg(II) by an extracelluar biopolymer poly(c-glutamic acid). Bioresour. Technol. 100, 200–207.
M. Kadota (Editor), Current Adsorption Technology, vols. 155–167, 1993, publication; United Engineering Center.
Kai, T., Yamamot, S., Kanagawa, Y., Ishihara, S., 2001a. Adsorption characteristics of Hg (II) on wood charcoal. Resour. Process. 48, 19–26.
Kai, T., Yamamot, S., Kanagawa, Y., Ishihara, S., 2001b. The adsorption characteristics of cadmium (II), lead (II), and mercury (II) in mixed aqueous solutions by wood charcoal. Resour. Process. 48, 158–167.
Khalid, N., Ahmad, S., Kiani, S.N., Ahimed, J., 1999. Removal of Hg from aqueous solutions by adsorption to rice husk. Separ. Sci. Technol. 34, 3139–3153.
Knocke, W.R., Hemphill, L.H., 1982. Mercury(II) sorption by waste rubber. Water Res. 15, 449–452.
Krishnan, K.A., Anirudhan, T.S., 2002. Removal of Hg(II) from aqueous solutions and chlor-alkali industry effluent by steam activated and sulphurised activated carbon prepared from bagasse pitch: kinetics and equilibrium studies. J. Hazard Mater. 92, 161–183.
Krishnani, K.K., Meng, Z., Christodoulatos, C., Boddu, V.M., 2008. Biosorption

mechanism of nine different heavy metals onto biomatrix from rice husk. J. Hazard Mater. 153, 1222–1234.
Li, H., Dong, X., da Silva, E.B., de Oliveira, L.M., Chen, Y., Ma, L.Q., 2017a. Mechanisms of metal sorption by biochars: biochar characteristics and modifications. Chemosphere 178, 466–478.
Li, H., Dong, X., Silva, E.B., Pliveria, L.M., Chen, Y., Ma, L.Q., 2017b. Mechanisms of metal sorption by biochars: biochar characteristics and modifications. Chemosphere 178, 466–478.
Liu, P., Ptacek, C.J., Blowes, D.W., Ladis, R.C., 2016. Mechanisms of mercury removal by biochars produced from different feedstocks determined using X-ray absorption spectroscopy. J. Hazard Mater. 308, 233–242.
Macchi, D.G., Marrani, M., Coretti, M.R., 1985. Optimization of mercury removal from chloralkali industrial wastewater by starch xanthate. Environ. Technol. Lett. 6, 369–380.
P. Miretxky, AF. Cirelli, Hg(II) removal from water by chitosan and chitosan derivatives: a review, J. Hazard Mater., 167, 2000, 10-23.
Mishra, S.P., Chaudhury, G.R., 1996. Kinetic of Zn^{2+} adsorption by Penicillium sp. Hydrometallurgy 40, 11–23.
Mochizuki, Y., Bud, J., Liu, J., Tsubouchi, N., 2020. Production of silicone tetrachloride from rice husk by chlorination and performance of mercury adsorption from aqueous solution of chlorinated residue. ACS Omega 5, 29110–29120.
Mochizuki, Y., Kubota, H., Uebo, K., Tsubouchi, N., 2019. Gasification of carbon/carbon composite prepared from pyrolyzed char of low-grade coke and low-rank coal. Powder Technol. 355, 782–792.
Nishi, S., Kobayashi, R., Horimot, Y., 1987. Mechanism of the coadsorption of mercury(II) and halogenide ions on activated carbon. Nippon Kagaku Kaishi 12, 1712–1717.
O'Connor, D., Peng, T., Li, G., Wang, S., Duan, L., Mulder, J., Cornelissen, G., Chang, Z., Yang, S., Hou, D., 2018. Sulfur-modified rice husk biochar: a green method or the remediation of mercury contaminated soil. Sci. Total Environ. 621, 819–826.
Rocha, C.G., Zaia, D.A., Alfaya, R.V.S., Alfaya, A.A.S., 2009. Use of rice straw as biosorbent for removal of Cu(II), Zn(II), Cd(II) and Hg(II) ions in industrial effluents. J. Hazard Mater. 166, 383–388.
Rocha, L.S., Lopes, C.B., Borges, J.A., Duarte, A.C., Pereira, E., 2013. Valuation of unmodified rice husk waste as an eco-friendly sorbent to remove mercury: a study using environmental realistic concentrations. Water Air Soil Pollut. 224, 1599.
Song, S.T., Saman, N., Johari, K., Mat, H.B., 2013. Removal of mercury(II) from aqueous solution by using rice residues. J. Teknol. 63, 67–73.
Tan, G., Sun, W., Xu, Y., Wang, H., Xu, N., 2016. Sorption of mercury(II) and atrazine by biochar, modified biochars and biochar based activated carbon in aqueous solution. Bioresour. Technol. 211, 727–735.
Tsubouchi, N., Mochizuki, Y., Ono, Y., Uebo, K., Takanohashi, T., Sakimoto, N., 2014. Sulfur and nitrogen distributions during coal carbonization and the influence s of these elements on coal fluidity. ISIJ Int. 54, 2439–2445.
Tsubouchi, N., Ohtaka, N., Ohtsuka, Y., 2016. Reactions of hydrogen chloride with carbonaceous materials and the formation of surface chlorine species. Energy Fuel. 30, 2320–2327.
Velempini, T., Pillay, K., 2019. Sulphur functionalized materials for Hg(II) adsorption: a review. J. Environ. Chem. Eng. 7, 103350.
Vikrant, K., Kim, H.-H., 2019. Nanomaterials for the adsorptive treatment of Hg(II) ions from water. Chem. Eng. J. 358, 264–282.
Wajima, T., Sugawara, K., 2011. Adsorption behaviors of mercury from aqueous solution using sulfur-impregnated adsorbent developed from coal. Fuel Process. Technol. 92, 1322–1327.
Xiao, B., Thomas, K.M., 2004. Competitive adsorption of aqueous metal ions on an oxidized nanoporous activated carbon. Langmuir 20, 4566–4578.
Xu, X., Schierz, A., Xu, N., Cao, X., 2016. Comparison of the characteristics and mechanisms of Hg(II) sorption by biochars and activated carbon. J. Colloid Interface Sci. 463, 55–60.
Yand, X., Wan, Y., Zheng, Y., He, F., Yu, Z., Huanf, J., Wang, H., Ok, Y.S., Jiang, Y., Gao, B., 2019. Surface functional groups of carbon-based adsorbents and their roles in the removal of heavy metals from aqueous solutions: a critical review. Chem. Eng. J. 366, 608–621.
Yoshida, H., Kamegawa, K., Arita, S., 1976. Mechanism of adsorption of mercury(II) ion on activated carbon. Nippon Kagaku Kaishi 5, 808–813.